RSC Advances

PAPER

View Article Online
View Journal | View Issue

Cite this: *RSC Adv.*, 2016, **6**, 93922

Smart-phone attachable, flow-assisted magnetic focusing device†

Reza Amin,[a] Stephanie Knowlton,[b] Bekir Yenilmez,[a] Alexander Hart,[b] Ashwini Joshi[b] and Savas Tasoglu*[ab]

Detection and sorting of particles and cells in a continuous flow stream is of great importance to downstream biological studies and high-throughput screening. Many particle separation techniques require peripheral devices, complex channel designs or setups that can limit the process and its applications. Here, we present a smart-phone attachable continuous flow magnetic focusing device as an inexpensive and portable tool for reproducible, real-time detection and sorting of particles in high-volume samples based on their volumetric mass density. Diamagnetic particles were suspended in a paramagnetic medium and pumped through a microcapillary located between two permanent magnets. Appropriate flow rate allows each particle to be confined at a vertical equilibrium height. A magnifying lens is placed between the smart-phone camera and capillary to capture images of micro-objects illuminated by an LED. A custom-developed Android application is used for adjusting the focal plane and other imaging parameters, and communicating with a microcontroller to control the pump and LED intensity. The effects of magnet length and flow rate on the particle sorting performance of the setup have been investigated. This device offers a portable, low-cost, digital, and versatile method for identifying, sorting, and quantifying particles on the basis of their volumetric mass densities.

Received 2nd August 2016
Accepted 12th September 2016

DOI: 10.1039/c6ra19483d

www.rsc.org/advances

Introduction

Density and magnetic susceptibility of any object are fundamental characteristics which are indicative of its internal properties. Magnetic focusing (or magnetic levitation), which involves suspending and confining objects in a paramagnetic fluid in the presence of a magnetic field, is proven to be an effective method for analyzing the density and the magnetic susceptibility of objects.[1,2] Previously, magnetic focusing has been used for density-based sorting of foods[1] and chemical[2] and biological micro-scale objects,[3,4] distinguishing atomic level differences in polymer chemical compositions, monitoring chemical reactions,[5] and measuring the binding of proteins to ligands.[6] This technology has also been leveraged for guiding objects to self-assembly[7,9–11] and noncontact orientation of objects.[8] Recently, a compact magnetic focusing platform compatible with fluorescence microscopes has been demonstrated for interrogation and monitoring of cells.[3] In another study, a small smart-phone attachable platform has been developed for handling small volumes of samples (10 μL) and on-site density measurements of micro-objects suspended in the volume.[9,10] Additionally, continuous flow magnetic focusing has been used for spatial sorting of both particles and live cells in a microscopy-compatible platform.[11]

Although magnetic focusing has been well studied for spatial sorting of particles, a portable approach without requiring peripheral devices and expensive imaging equipment to detect and sort particles in high-volume samples has not yet to be developed. For instance, rare micro-object isolation requires high volume sample handling (*e.g.* 5–10 mL sample for circulating tumor cell detection, unlike point-of-care finger-prick blood analysis which may be used for certain blood disorder diagnoses, *i.e.* 10 μL [3,9]). Rare micro-object isolation and characterization have a wide range of scientific, clinical, public health, safety and commercial applications.[12] Examples include detection of pathogenic bacteria in food,[13] rare antigen-specific lymphocytes,[14] circulating endothelial cells (CECs) in blood,[15,16] hematopoietic stem cells (HSCs) in blood,[17,18] and circulating tumor cells (CTCs).[19] As a notable example, to isolate circulating tumor cells (CTCs), the sample is pumped through antibody-coated microfluidic chips that interact with CTCs and trap them.[20] Therefore, portable and inexpensive tools for real-time characterization and monitoring of rare micro-objects would positively impact many chemical and biological fields.

The increase in cellphone subscriptions all around the globe,[21] advancements in cellphones' capabilities (*e.g.* high performance imaging and computation power), as well as their cost-effective, portable and compact features, have made

[a]*Department of Mechanical Engineering, University of Connecticut, Storrs, CT 06269, USA. E-mail: savas@engr.uconn.edu*

[b]*Department of Biomedical Engineering, University of Connecticut, Storrs, CT 06269, USA*

† Electronic supplementary information (ESI) available. See DOI: 10.1039/c6ra19483d

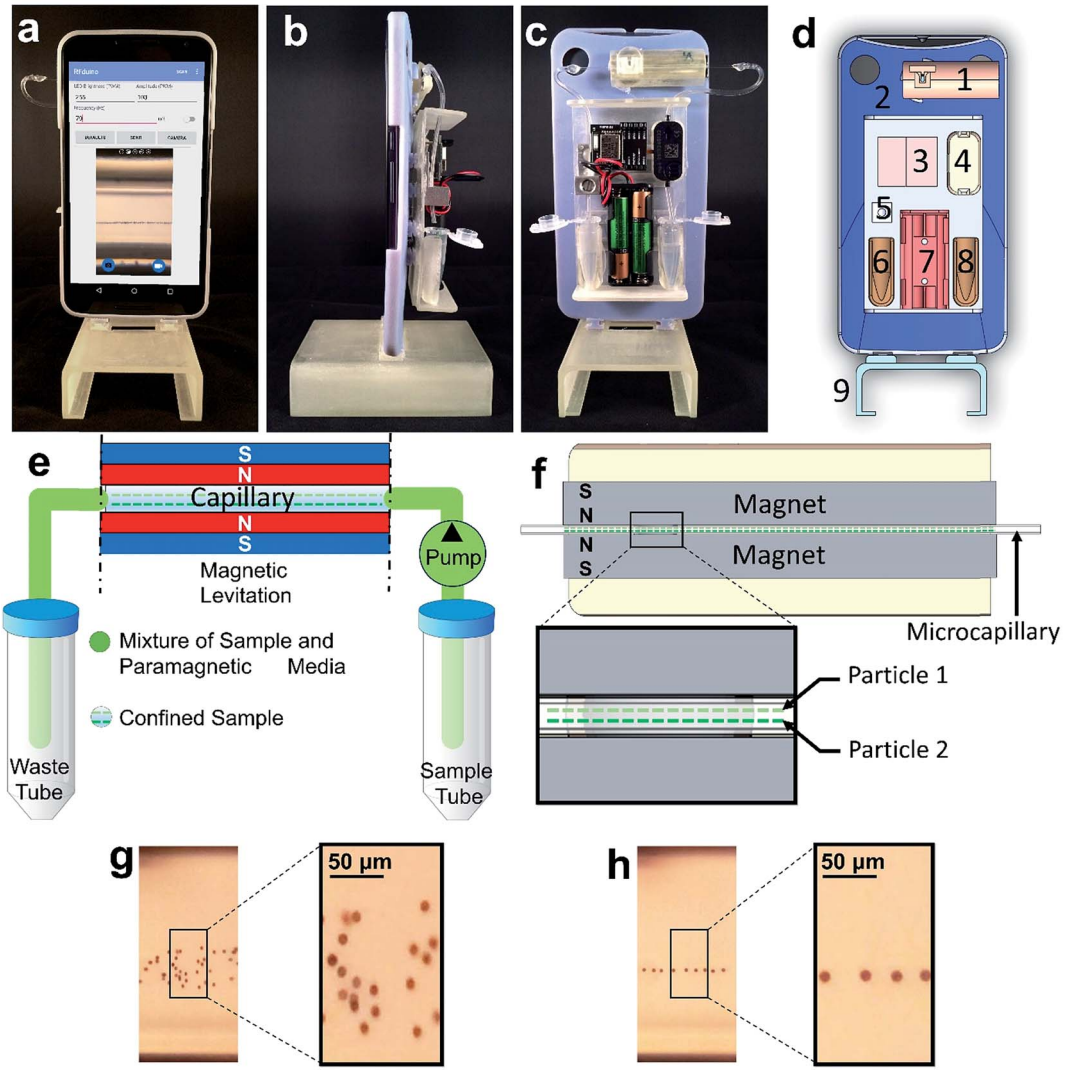

Fig. 1 Smart-phone attachable, flow-assisted magnetic focusing device. (a–c) Front (a), side (b), and back (c) views of smart-phone-compatible flow-integrated magnetic focusing setup. (d) The components of the device: (1) magnetic focusing module, including permanent magnets, square microcapillary, lens, LED and light diffuser, (2) cellphone case, (3) electronics, including the microcontroller, pump driver, and Bluetooth receiver, (4) micro-pump holder, (5) adjustable orifice, (6) waste tube holder, (7) AAA battery holder, (8) sample tube holder, (9) dual-purpose stand and cover. (e) Schematic of the flow-assisted magnetic focusing device. (f) Cross-section of magnetic focusing module. (g) Distribution of the beads flowing through the magnetic field (4 cm magnet length) at a rate of ~0.85 μL s^{-1} (beads have not reached equilibrium). (h) Confinement of beads flowing through the magnetic field (4 cm magnet length) at a rate of ~0.085 μL s^{-1} (beads have reached equilibrium).

cellphones a promising platform for various point-of-care diagnosis tools.[22,23] Here, we report a smart-phone based magnetic focusing device for reproducible, real-time monitoring, sorting, and digital quantification of particles in high-volume samples. To apply the magnetic focusing technique on large sample volumes, the sample is pumped through a magnetic field and simultaneously imaged. The flow rate is adjusted so that the time for the particles crossing the magnetic field is longer than the equilibrium time.[24] To achieve such precise flow rates, this device includes a microcontroller connected to an Android application to drive an embedded piezoelectric micro-pump. The device's agile micro-object spatial sorting allows monitoring of high-volume (milliliter-scale) samples that are continuously pumped in highly laminar flow through the magnetic focusing unit (Fig. 1a–c).

Methods

Materials

Reagents and materials. Gadolinium-based paramagnetic medium, Gadavist (Bayer, Whippany NJ 07981); VitroTubes square capillary microcells, borosilicate glass, 100 mm (8270-100, Vitrocom, Mountain Glass, NJ, USA); 1.5 mL Eppendorf™ snap-cap microcentrifuge Safe-Lock™ tubes (0540225, Fisher Scientific International, Inc., Hampton, New Hampshire, USA); Transparent Tygon® tubing, inner diameter of 1.02 mm (mp-t, Bartels Mikrotechnik GmbH, Dortmund, Germany); N52-grade nickel plated NdFeB magnets (50.8 × 2 × 5 mm^3), magnetized through the 5 mm thickness (custom design, K&J Magnetics, Inc., Pipersville, PA, USA); aspheric lens, diameter of 6.33 mm, numerical aperture 0.64 mm (Edmund Optics, Barrington, NJ,

USA); LED Luxeon warm white 3000K 3SMD (LXW9-PW30, Aachen, Germany); unmounted N-BK7 ground glass diffuser, 1500 Grit (DG05-1500, Thor Labs, Newton, NJ, USA); 3D printer resin, transparent PolyJet photopolymer (RGD720, Stratasys, Eden Prairie, Minnesota, USA).

Electronic components. Rechargeable AAA battery (Duracell, Bethel, CT, USA); mp6 micro-pumps (mp6, Bartels Mikrotechnik GmbH, Dortmund, Germany); mp6-OEM driver module for micro-pumps (mp6-OEM, Bartels Mikrotechnik GmbH, Dortmund, Germany); wireless enabled microcontroller (RFD22102, RFduino, Hermosa Beach, CA, USA); Nexus 6 smartphone (Motorola, Illinois, USA).

Design and fabrication of the setup *via* 3D printer

Different components of the smart-phone apparatus have been modularly designed in computer-aided design software, Solidworks (Dassault Systèmes, Vélizy-Villacoublay, France) (ESI Fig. 1†), including the cellphone case, stand, micro-pump holder, sample and waste tube holders, AAA battery holder and magnetic focusing module. The 3D model of the device was printed with an Objet30 prime 3D printer (Stratasys, Eden Prairie, Minnesota, USA) using the transparent PolyJet photopolymer and opaque VeroBlue photopolymer.[29,30] In order to hold the setup vertically upright, we designed a dual-purpose stand which functions both as a stand and cover for the micro-pump, electronics, and sample holders after the analysis (ESI Fig. 1e–g†). The magnetic focusing module contains horizontal slots for two NdFeB magnets with the same poles facing each other and a microcapillary (glass square capillary tubing) between them with a clearance of 0.1 mm from each side. The magnetic focusing module is attached to the cellphone case using a circular slot joint. To achieve the microscopic imaging of particles in the magnetic field, the magnetic module has a circular slot along the optical axis of the built-in smart-phone camera which holds an aspheric lens between the camera and the sample (microcapillary). To illuminate the sample, a LED is placed at the opposite end of the sample and aligned with the circular slot. A light diffuser is used between the LED and the sample to collimate the light for higher quality imaging. The micro-pump pumps the sample from a sample reservoir to one end of the microcapillary through the tubing, which then passes through the magnetic field and microscopic imaging setup, and finally drains to the waste tube through additional tubing. An orifice is used to fine tune the flow rate by adding an adjustable resistance to the outlet tubing. The complete setup is illustrated in Fig. 1.

Integration of electronic components

The smart-phone apparatus contains a wireless-enabled microcontroller that communicates with the smart-phone through a Bluetooth wireless module. The microcontroller receives the set points of micro-pump flow rate (in terms of input amplitude and frequency of the micro-pump) and LED intensity from the smart-phone user interface. Then, it generates the appropriate outputs for the micro-pump controller and LED in order to achieve the set points. Two serially-connected AAA rechargeable batteries work as a 3 volt-DC power supply for the apparatus. The micro-pump driver receives the amplitude (as a PWM signal equivalent to 0–3 volt DC) and frequency (as a 0–100 Hz square signal) set points from microcontroller and generates the micro-pump driving signal that ranges between 0–250 volts in amplitude and 0–100 Hz in frequency. An Android application has been developed that plays the roles of a user interface and an image processing tool of the apparatus.

Bluetooth service

A Bluetooth low energy (BLE) service was implemented and handled on the smart-phone side while the RFduino carried out the commands sent from the application. BLE provides efficient communication between two devices while requiring less power and maintaining a high rate of data transfer. BLE services run at a frequency of 2.4 GHz with 40 channels having equal spacing of 2 MHz. Currently, all of the BLE profiles are based on GATT (generic attribute profile), providing an organized hierarchy of data with different tags, which could belong to two separate devices. This system defines the simplest piece of data as a characteristic which is then bundled into larger structures called services. A BLE connection typically has a client and one or more servers, with a client initiating any GATT requests, while the server responds. In this case, the GATT server was the RFduino and the client was the smart-phone. The connection was implemented as a service on the smart-phone to allow for a continuous connection over the application's lifecycle. The data collected from the user interface was bundled and sent across the BLE service with a universally unique identifier (UUID) tied to the data. On the server-side (RFduino), this data was received and unbundled and the information was sent to the respective pins on the board.

Smart-phone application

The application targets Android devices running a minimum requirement of SDK 21, or Android 5.0 (LOLLIPOP). This is to allow the use of the Camera2 application program interface (API) which permits more control over the previous Camera API, giving the ability to change the focal distance, ISO settings, white balance levels, and much more. Because of this requirement, backward compatibility is very limited for phones not supporting Camera2. The communication to the pump was done through the BLE API (introduced in Android 4.3) and an RFduino microcontroller.

Ethical statement

Approval: Human blood samples were obtained *via* fingerstick in accordance with relevant University of Connecticut guidelines and regulations. All experimental protocols were approved by the University of Connecticut, Institutional Review Board (IRB) Office. *Protocol #H15-048*: "Acquisition of Human Blood Samples for Optical Imaging in a Smart-phone-Compatible Apparatus". *Accordance*: The methods were carried out in accordance with the approved UCONN guidelines. *Informed consent*: Informed consent was obtained from all subjects.

Results and discussion

Modeling of the magnetic field

The magnetic field generated by the two permanent magnets was analytically solved using Matlab (Fig. 2).[3,9,25] Magnetic focusing of particles suspended in a paramagnetic medium and flowing through the magnetic field can be described as a combination of four forces. The gravitational force (F_g) is due to the object's buoyancy, or density relative to that of the medium. This force is upward in the case of a particle less dense than the medium and downward in the case of a particle denser than the medium. The magnetic force (F_m) is due to the object's low magnetic susceptibility relative to the medium with directionality toward the center between the magnets. This force is strongest near the surface of the magnets and approaches zero at the center line between the magnets (Fig. 2b). Thus, in the

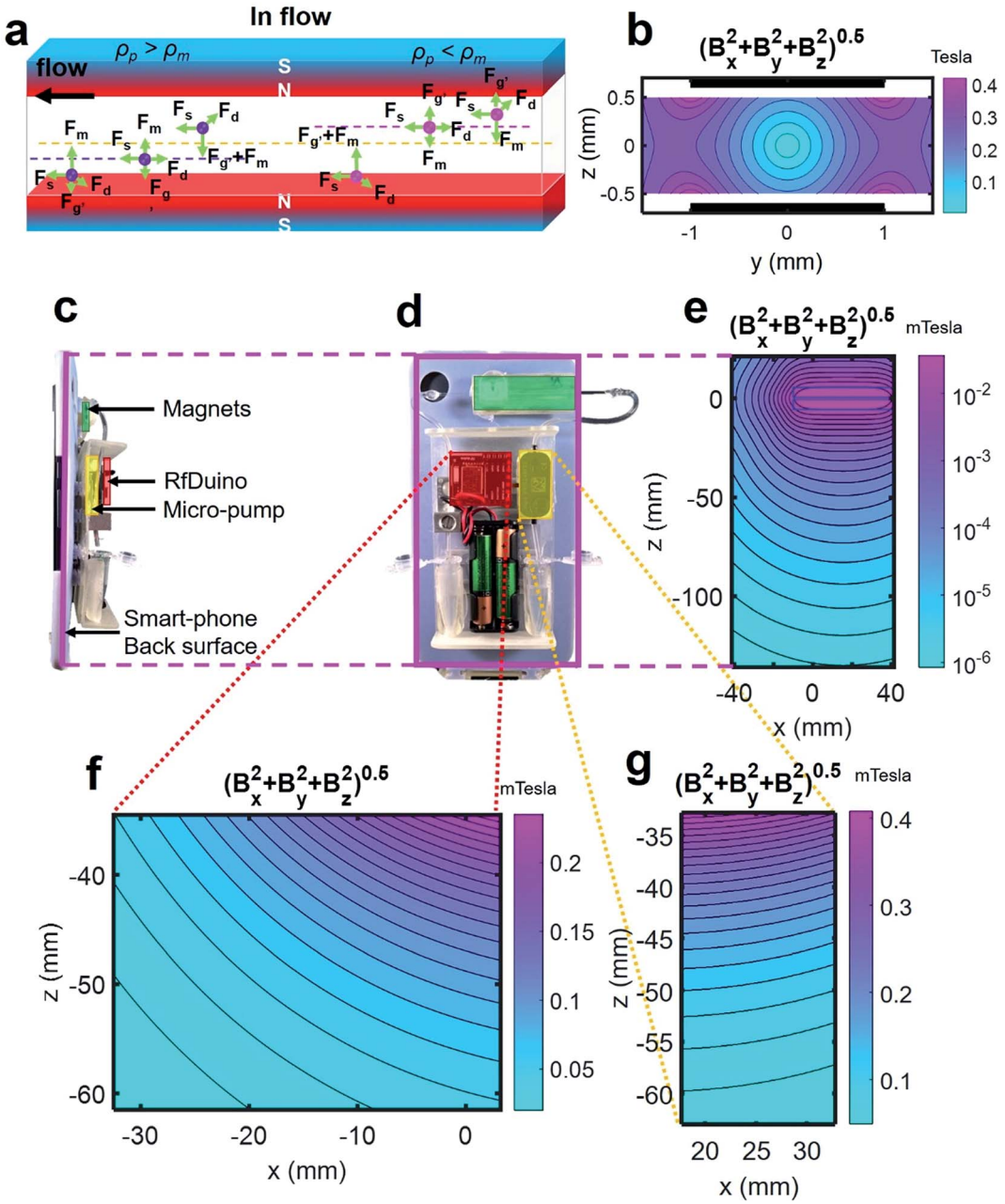

Fig. 2 Magnetic field at various sections. (a) Forces acting on the beads under flow, including gravitational force due to the object's buoyancy (F_g), magnetic force due to the object's low magnetic susceptibility relative to the medium (F_m), shear force (F_s) due to the fluid flow, and drag force (F_d) opposing the motion of the particle. Purple spheres represent micro-objects which are denser than the suspending medium and pink spheres represent micro-objects which are less dense than the suspending medium. (b) The magnitude of the net magnetic force at the magnet cross-section (flow direction is normal to the cross-section, showing that field strength is lowest at the center of the micro-capillary). (c–d) Labeled and color-coded components shown from the (c) side and (d) back surfaces. (e–g) Magnetic force acting on the back surfaces of (e) the smart-phone (as shown in (c)), (f) microcontroller board (as shown in (d) in red), and (g) micro-pump (as shown in (d) in yellow).

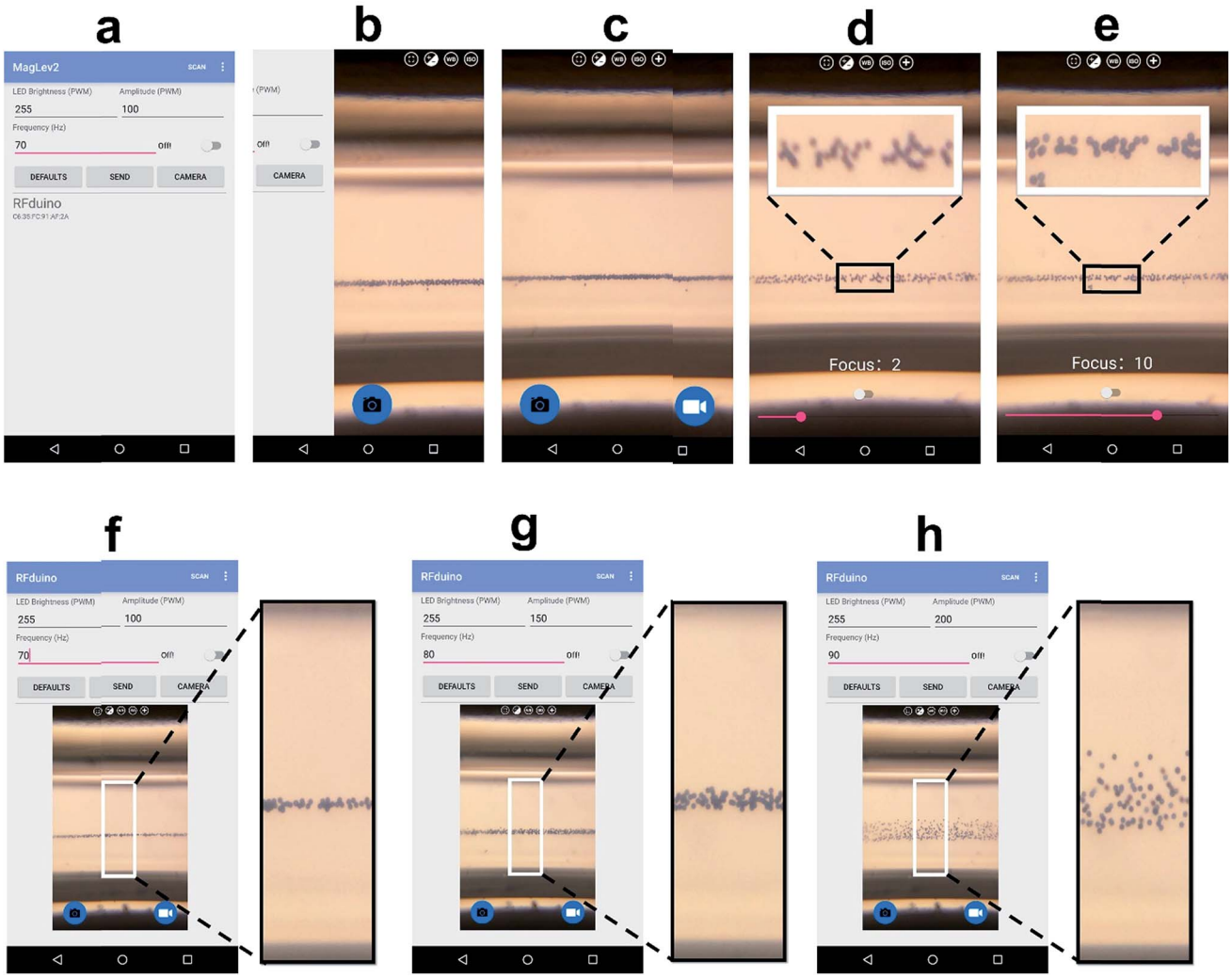

Fig. 3 Smart-phone application for magnetic focusing pump and camera support. (a) Initial home screen presented to the user with options for adjusting the LED brightness, amplitude, and frequency of the signal sent to the pump. The user can scan for Bluetooth devices within range which are presented on the bottom half of the screen; (b and c) a swipe to the left will reveal the full-screen camera. This will have buttons for taking a picture and video as well as controls for altering the focal distance, zoom, ISO, and other options. (d and e) By selecting the focal distance button, the user will be able to alter the focal distance to reach the best focus of the micro-objects. The objects in (d) are not in focus and the objects in (e) are in focus. (f–h) Changing the amplitude and frequency of the pump. (f) The amplitude and frequency are chosen to be 100 PWM and 70 Hz respectively, resulting in confinement of the micro-objects (g) the amplitude and frequency are chosen to be 150 PWM and 80 Hz respectively, resulting in a flow rate higher than (f) and the beads being more distributed around the equilibrium line. (h) The amplitude and frequency are chosen to be 200 PWM and 90 Hz respectively, resulting in a flow rate higher than (f and g) and the beads being more spread around equilibrium line.

static case (no flow), a particle will move vertically to find equilibrium between F_g and F_m. As the particle moves toward equilibrium, it experiences a drag force (F_d) opposing the motion of the particle. Finally, in the case where pressure is applied to drive fluid flow, shear force (F_s) is also present, acting in the horizontal direction. Additionally, we solved analytical equations, as we described in our previous work,[10] to demonstrate the magnetic field strengths created by magnets and applied on the critical components of our setup. The magnetic field was plotted at the locations of each of the electrical components: the smart-phone (Fig. 2e), the microcontroller (Fig. 2f), and the pump (Fig. 2g). The total magnetic field on all components was below 0.4 mTesla, which is less than that of a typical refrigerator magnet and does not cause any noticeable interference with the proper function of the smart-phone.

Smart-phone application and imaging

The smart-phone application provides a simple user interface for controlling the fluid flow as well as capturing images (Fig. 3). The application allows the user to specify the brightness of the LED illumination (with a value between 0 and 255) and to control the Bluetooth communication from this interface (Fig. 3a). After sending the desired parameters to the pumping components, the user can easily switch to imaging mode and manually focus the camera on the micro-objects as well as

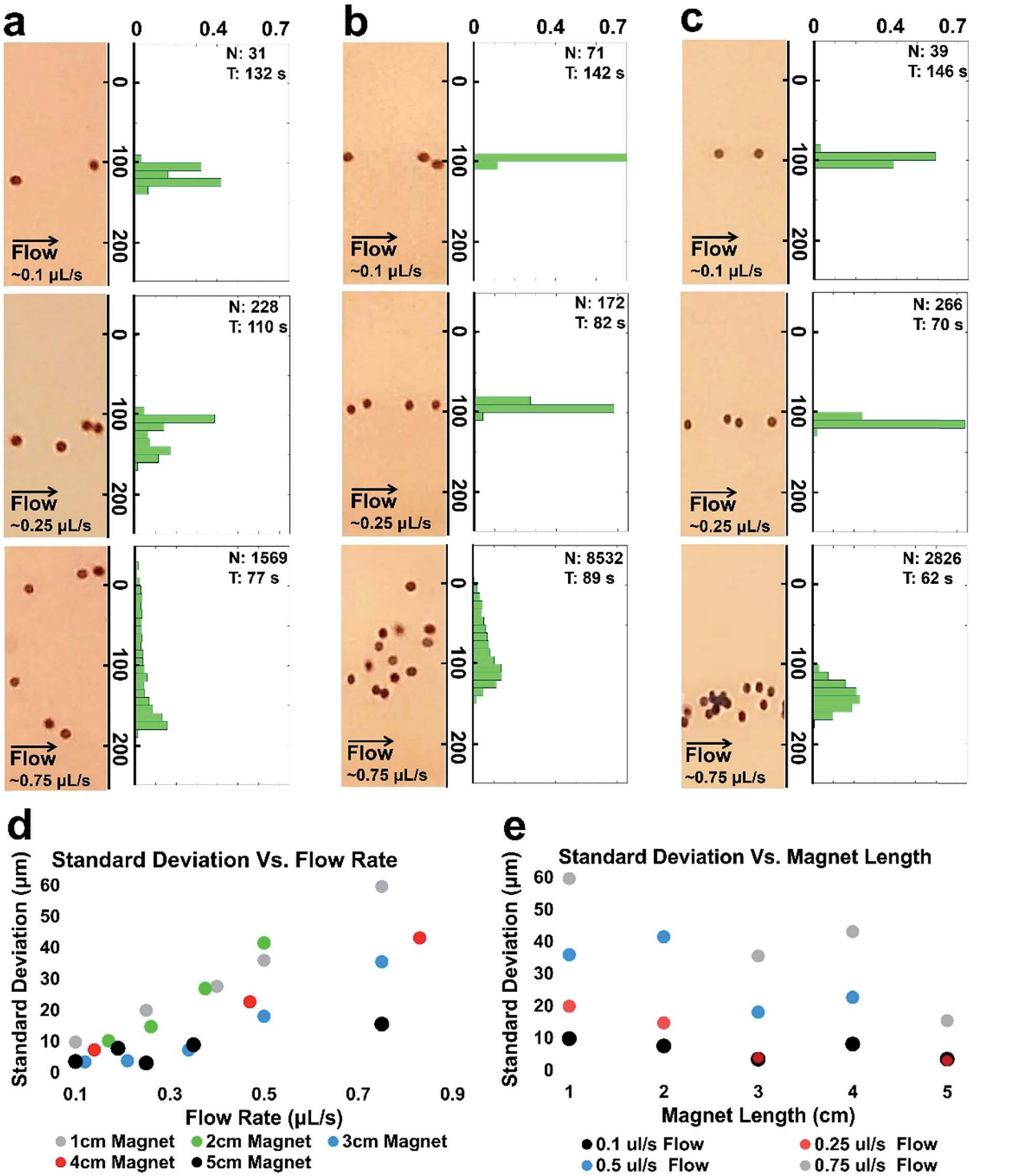

Fig. 4 Micro-object focusing at different flow rates and a range of magnet lengths. (a–c) Histogram of microsphere distribution within the magnetic field of 1 cm (a), 3 cm (b), and 5 cm (c) magnet length, while flow is on for 1 minute 30 seconds on average (total elapsed time stamps (*T*) and total counted number of particles (*N*) are given at the inset of each histogram). Capillary width is 700 µm (*i.e.*, −350 represents the top of the capillary and 350 represents the bottom of the capillary in the vertical axis of histograms). At lower flow rates, the Gaussian distribution fit to the data has a slightly higher standard deviation. Similarly, at lower magnet lengths, the Gaussian distribution has a greater standard deviation than at greater magnet lengths. (d) Standard deviation of micro-object confinement *versus* flow rate at various magnet lengths. (e) Standard deviation of micro-object confinement *versus* magnet length at various flow rates.

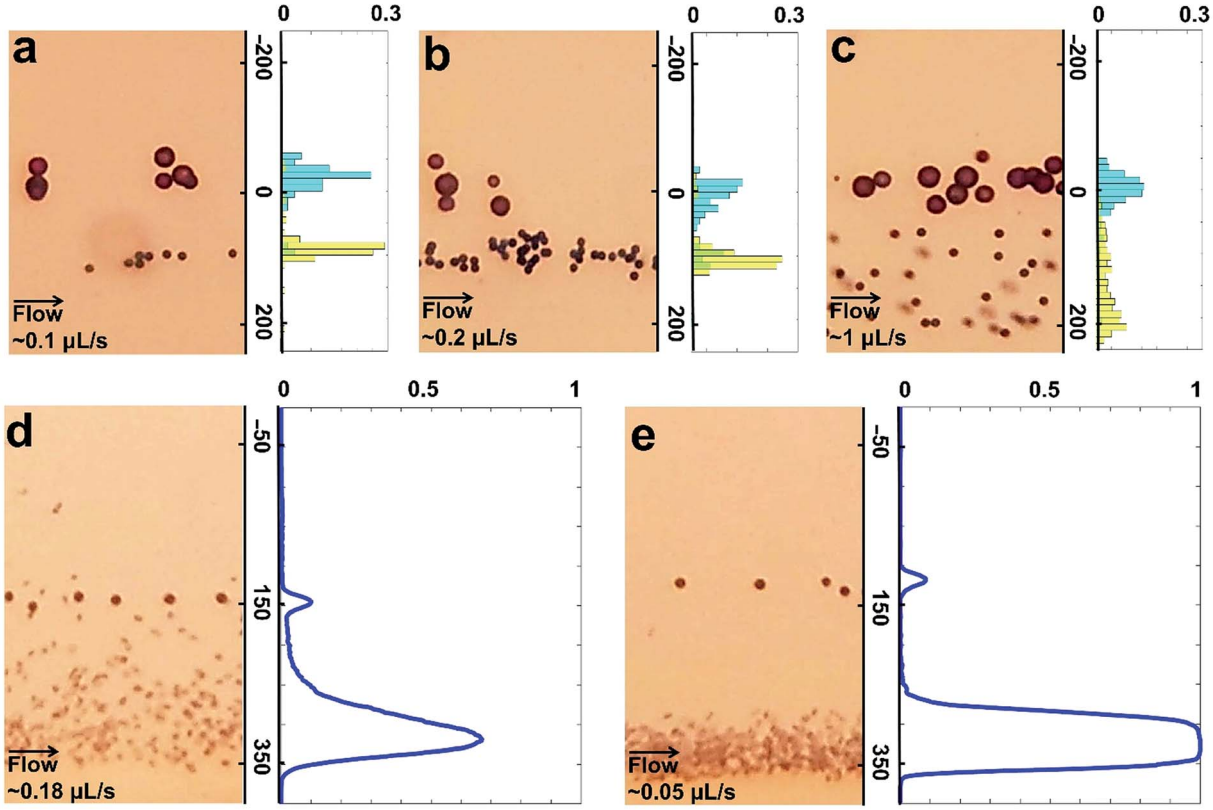

Fig. 5 Sorting of blood cells and particles at low and high flow rates. (a–c) Images of the microspheres from the cellphone screen and corresponding distribution of two micro-objects of different known densities suspended in the same sample at (a) 0.1 μL s^{-1}, (b) 0.2 μL s^{-1}, and (c) 1 μL s^{-1}. The blue histogram distribution represents the focusing height of the 0.97 g cm^{-3} microspheres and the yellow histogram distribution represents the 1.12 g cm^{-3} microspheres. (d and e) Images of the microspheres from cell phone screen and blood cells, and corresponding summed and normalized pixel intensities of micro-objects and blood cells flowed at (d) 0.18 μL s^{-1} and (e) 0.05 μL s^{-1}. Relatively low numbers of microspheres compared to blood cells demonstrates the rare particle detection and sorting capability.

adjust other imaging parameters (Fig. 3b–e). The user can also adjust the amplitude and frequency driving the pump which are positively correlated with the flow rate (Fig. 3f–h and ESI Fig. 2 and 3†).

Effects of flow rate and magnet length on micro-object confinement

Since the flow rate dictates the time that particles remain in the magnetic field and affects the confinement rate of particles, the effect of flow rate has been investigated. 10 μm polystyrene microspheres were suspended in a 50 mM concentration gadolinium-based paramagnetic medium (Gadavist). The solution was pumped between the permanent magnets in the magnetic focusing module with flow rates of 0.1, 0.25 and 0.75 μL s^{-1}. Since the length of the magnet and flow rate determine the magnetic forces and exposure time to these forces by micro-objects, the flow experiments have been performed for a range of magnet lengths: 10, 20, 30, 40 and 50 mm.

Fig. 4a–c shows the distribution of 10 μm polystyrene microspheres suspended in a 50 mM Gadavist solution and pumped at different flow rates. At a 0.1 μL s^{-1} flow rate and 50 mm magnet length, over 95% of the particles were confined to a band with a width of 14 μm (which is ±2 μm around a single microsphere size, *i.e.* 10 μm). As the flow rate was increased to ~0.25 μL s^{-1} and ~0.75 μL s^{-1}, the microspheres remained for a shorter time in the magnetic field (*i.e.* exposed to magnetic forces for a shorter time) and thus attained a wider distribution of microspheres around the equilibrium line. Fig. 4d shows that for all magnet lengths, increasing the flow rate increases the standard deviation of microsphere's distribution (wider distribution).

The results shown in Fig. 4a–c indicate that 95% of the particles were confined to their equilibrium at a 0.1 μL s^{-1} flow rate and 50 mm magnet length. Decreasing the length of the magnets results in a wider distribution of microspheres around the equilibrium line. Fig. 4e shows that, for all flow rates tested, increasing the magnet length decreases the standard deviation of the microsphere's distribution (more confinement). However, it should be noted that the strength of the magnetic field between the permanent magnets varies throughout the length of the magnets and is at its maximum at the two ends of magnets. Therefore, magnets should be perfectly aligned at their ends to avoid any abrupt changes in the focusing height of the particles as they leave the magnetic field.

Density-based sorting of multiple micro-objects

To demonstrate sorting capability of our approach for heterogeneous mixtures of particles suspended in the same sample, we first used two microspheres: one with a volumetric mass density of 0.97 g cm^{-3} and the other with a volumetric mass density of 1.12 g cm^{-3}. Fig. 5a–c demonstrates sorting of particles on the basis of their volumetric mass densities. At lower flow rates, *e.g.* 0.1 μL s^{-1} and 0.2 μL s^{-1}, the particle sorting was more efficient. Around 10% overlap between the particle distributions across the width of capillary was observed at a flow rate of 0.1 μL s^{-1}. At the highest flow rate, the separation between the distributions was less distinct, with 25% overlap due to less exposure to the magnetic field and thus magnetic forces.

Fig. 5d & e demonstrate the magnetic focusing of blood samples obtained *via* fingerstick and the sorting of the cells from microspheres at flow rates of 0.18 μL s^{-1} (Fig. 5d) and 0.05 μL s^{-1} (Fig. 5e). Results show that blood cells take a longer time to equilibrate than microspheres. Sorting was achieved without overlap between distributions at 0.05 μL s^{-1} (Fig. 5e). Relatively much lower numbers of microspheres compared to red blood cells in Fig. 5d and e also demonstrate the rare particle detection and sorting capability of this approach.

Conclusions

We have developed a flow-assisted smart-phone attachable magnetic focusing device for real-time detection and quantification of particles in high-volume samples. The device relies on magnetophoresis to confine and sort particles on the basis of their volumetric mass densities, where denser objects equilibrate at a lower height than less dense objects. The device is a simple and versatile platform which employs permanent magnets and a Bluetooth-enabled micro-pump system which communicates to a smart-phone through a custom-developed Android application. The system flows the sample through a microcapillary in front of a magnifying lens to allow images of confining particles to be captured using the built-in camera of a smart-phone. We have investigated the performance of the flow-assisted magnetic focusing device by quantifying the normalized particle count across the capillary width (*i.e.* probability of a particle to flow at a distance across the capillary width). The results show that the confinement of particles can be controlled by altering the flow rate generated by the micropump and the flow distance through the permanent magnets.

We have previously demonstrated diagnosis of sickle cell anemia using a smart-phone-based magnetic focusing in a static (no-flow) setup handling only small volumes of sample (up to tens of microliters of sample).[9,10] Unlike the setup in,[9,10] the presented flow-assisted device here handles large volumes of sample *via* an integrated and optimized miniature pump for biological applications and embedded control unit (*i.e.* milliliters of sample >100 folds of sample volumes achieved in our previously presented setup).[9,10] The capability of handling large volumes of sample in a portable device is critical especially for rare cell or microparticle identification and purification applications in resource-limited settings. Additionally, we have developed a new software application to dynamically control the internal lens embedded in the smart-phone and its location with respect to sample, which was not possible in.[9,10] This smart-phone application provides the user with additional capabilities and flexibilities in resource-limited settings such as dynamic and on-demand control over focal length and better imaging of the sample.

We have demonstrated the sorting and confinement of particles of two different densities at predicable locations in the magnetic field. This distinct sorting may also be leveraged in future studies to isolate the particles of different densities by leveraging a microfluidic separator at the end of the magnetic field. Further, particles of a single density could be concentrated in the sample by separating the stream of confined beads from the surrounding medium. Lower flow rates have more confinement of particles but result in a lower volume throughput, which can be a drawback for rare object detection in high-volume samples. This limitation can be addressed by integrating multiple passes in the magnetic field or by using longer magnets. The viscosity of the sample solution does not affect the sorting resolution as the equilibrium height does not depend on viscosity, for flow-free magnetic focusing.[3] On the other hand, an increase in viscosity would cause an increase in the equilibrium time for flow-assisted magnetic focusing (*i.e.* total elapsed time for particles to reach equilibrium) due to the amplified drag forces. An increase in viscosity would slow down the motion of cells and particles towards their equilibrium point. Therefore it would require either a longer magnetic field exposure time or a smaller flow rate to be able to achieve a similar sorting resolution.

The cells, or particles used in our study have negligible magnetic susceptibilities compared to the suspending paramagnetic solution that we employed (*i.e.* Gadavist). The magnets in use today in MRI for human research are in the 0.5 Tesla to 3.0 Tesla range, while the magnets we used in our setup are 0.375 Tesla. The paramagnetic solution, Gadavist, used for all experiments is currently employed for MRI investigations in humans and FDA approved. This medium is nontoxic, isoosmolar at the concentration used for imaging, and fully compatible with human blood cells.[3]

Future applications of the flow-assisted magnetic focusing approach include detection of biological components which are distinguished by density. Certain cell types, cells which are undergoing cell death, and diseased cells[3] have all been shown to have unique density signatures and thus distinct magnetic patterns, and can therefore be quantified and separated, even in low numbers, using this platform. Such applications of this low-cost and user-friendly device will have a significant impact in point-of-care high-throughput disease diagnostics, particularly in low-resource areas where advanced testing procedures are inaccessible. S.K. acknowledges that this material is based upon work supported by the National Science Foundation Graduate Research Fellowship (DGE-1247393). A provisional patent entitled "Magnetic Levitation with On-Board Optical Imaging and Image Analysis for Density-Based Separation, Identification,

and Measurement" has been filed with UCONN Case No. 16–027 on the technology described here. S.T. and S.K. disclose a financial interest in a startup company, mBiotics, related to the technology described here.

Third party rights

There is no material that we do not own the intellectual property.

Acknowledgements

ST acknowledges the American Heart Association Scientist Development Grant (15SDG25080056) and the University of Connecticut Research Excellence Program award for financial support of this research.

References

1 B. Yenilmez, S. Knowlton, C. H. Yu, M. M. Heeney and S. Tasoglu, Label-Free Sickle Cell Disease Diagnosis using a Low-Cost, Handheld Platform, *Advanced Materials Technologies*, 2016, **1**(5), 1600100.
2 B. Yenilmez, S. Knowlton and S. Tasoglu, Self-Contained Handheld Magnetic Platform for Point of Care Cytometry in Biological Samples, *Advanced Materials Technologies*, 2016.
3 K. A. Mirica, *et al.*, Magnetic levitation in the analysis of foods and water, *J. Agric. Food Chem.*, 2010, **58**(11), 6565–6569.
4 K. A. Mirica, *et al.*, Measuring densities of solids and liquids using magnetic levitation: fundamentals, *J. Am. Chem. Soc.*, 2009, **131**(29), 10049–10058.
5 S. Tasoglu, *et al.*, Levitational image cytometry with temporal resolution, *Adv. Mater.*, 2015, **27**(26), 901–3908.
6 A. B. Subramaniam, *et al.*, Metal-Amplified Density Assays, (MADAs), including a Density-Linked Immunosorbent Assay (DeLISA), *Lab Chip*, 2015, **15**(4), 1009–1022.
7 K. A. Mirica, *et al.*, Using magnetic levitation to distinguish atomic-level differences in chemical composition of polymers, and to monitor chemical reactions on solid supports, *J. Am. Chem. Soc.*, 2008, **130**(52), 17678–17680.
8 N. D. Shapiro, *et al.*, Magnetic Levitation as a Platform for Competitive Protein–Ligand Binding Assays, *Anal. Chem.*, 2012, **84**(14), 6166–6172.
9 S. Tasoglu, C. H. Yu, V. Liadudanskaya, S. Guven, C. Migliaresi and U. Demirci, Magnetic Levitational Assembly for Living Material Fabrication, *Adv. Healthcare Mater.*, 2015, **4**(10), 1469–1476.
10 S. Tasoglu, C. H. Yu, H. I. Gungordu, S. Guven, T. Vural and U. Demirci, Guided and magnetic self-assembly of magnetoceptive gels, *Nat. Commun.*, 2014, **5**, 4702.
11 S. Tasoglu, D. Kavaz, U. A. Gurkan, S. Guven, P. Chen, R. Zheng and U. Demirci, Paramagnetic Levitational Assembly of Hydrogels, *Advanced Materials*, 2013, **25**(8), 1137–1143.
12 K. A. Mirica, *et al.*, Using Magnetic Levitation for Three Dimensional Self-Assembly, *Adv. Mater.*, 2011, **23**(36), 4134–4140.
13 A. B. Subramaniam, *et al.*, Noncontact orientation of objects in three-dimensional space using magnetic levitation, *Proc. Natl. Acad. Sci. U. S. A.*, 2014, **111**(36), 12980–12985.
14 S. Knowlton, C. H. Yu, N. Jain, I. C. Ghiran and S. Tasoglu, Smart-Phone Based Magnetic Levitation for Measuring Densities, *PLoS One*, 2015, **10**(8), e0134400, DOI: 10.1371/journal.pone.0134400.
15 S. M. Knowlton, *et al.*, Sickle cell detection using a smartphone, *Sci. Rep.*, 2015, **5**, 15022.
16 A. I. Rodríguez-Villarreal, *et al.*, Flow focusing of particles and cells based on their intrinsic properties using a simple diamagnetic repulsion setup, *Lab Chip*, 2011, **11**(7), 1240–1248.
17 M. Zborowski and J. J. Chalmers, Rare cell separation and analysis by magnetic sorting, *Anal. Chem.*, 2011, **83**(21), 8050–8056.
18 C. Mu, *et al.*, Detecting low concentration bacterial cells in complex media using a microchip-based flow cytometer, *Sens. Actuators, B*, 2014, **202**, 1051–1057.
19 P. Bacher and A. Scheffold, Flow-cytometric analysis of rare antigen-specific T cells, *Cytometry, Part A*, 2013, **83**(8), 692–701.
20 S. Li, *et al.*, An Integrated Platform for Isolation, Processing and Mass Spectrometry-based Proteomic Profiling of Rare Cells in Whole Blood, *Mol. Cell. Proteomics*, 2015, **14**(6), 1672–1683.
21 J. A. Mund, *et al.*, Flow cytometric identification and functional characterization of immature and mature circulating endothelial cells, *Arterioscler., Thromb., Vasc. Biol.*, 2012, **32**(4), 1045–1053.
22 E. Ozkumur, *et al.*, Inertial focusing for tumor antigen-dependent and -independent sorting of rare circulating tumor cells, *Sci. Transl. Med.*, 2013, **5**(179), 179ra47.
23 R. T. Krivacic, *et al.*, A rare-cell detector for cancer, *Proc. Natl. Acad. Sci. U. S. A.*, 2004, **101**(29), 10501–10504.
24 J. H. Kang, *et al.*, A combined micromagnetic-microfluidic device for rapid capture and culture of rare circulating tumor cells, *Lab Chip*, 2012, **12**(12), 2175–2181.
25 S. Nagrath, *et al.*, Isolation of rare circulating tumour cells in cancer patients by microchip technology, *Nature*, 2007, **450**(7173), 1235–1239.
26 A. Arpa, *et al.*, Single lens off-chip cellphone microscopy, in *2012 IEEE Computer Society Conference on Computer Vision and Pattern Recognition Workshops (CVPRW)*, 2012.
27 H. Zhu, *et al.*, Optical imaging techniques for point-of-care diagnostics, *Lab Chip*, 2013, **13**(1), 51–67.
28 S. K. Vashist, *et al.*, Cellphone-based devices for bioanalytical sciences, *Anal. Bioanal. Chem.*, 2014, **406**(14), 3263–3277.
29 R. Amin, S. Knowlton, A. Hart, B. Yenilmez, F. Ghaderinezhad, S. Katebifar, M. Messina, A. Khademhosseini and S. Tasoglu, 3D-printed microfluidic devices, *Biofabrication*, 2016, **8**(2), 022001.

30 S. Knowlton, C. H. Yu, F. Ersoy, S. Emadi, A. Khademhosseini and S. Tasoglu, 3D-printed microfluidic chips with patterned, cell-laden hydrogel constructs, *Biofabrication*, 2016, **8**(2), 025019.
31 A. Winkleman, *et al.*, Density-based diamagnetic separation: devices for detecting binding events and for collecting unlabeled diamagnetic particles in paramagnetic solutions, *Anal. Chem.*, 2007, **79**(17), 6542–6550.
32 E. P. Furlani, *Permanent Magnet and Electromechanical Devices – ScienceDirect*, ed. I. Mayergoyz, Academic Press, New York, NY, 2001.